Journal of Multidisciplinary Engineering Science Studies (JMESS)
ISSN: 2458-925X
Vol. 6 Issue 2, February - 2020

Numerical Study Of The Heat Transfer Enhancement Inside An Internally Helical Grooved Tubes Containing Twisted Tape Inserts

[1]Taye S. Mogaji,
[1]Department of Mechanical Engineering, Federal University of Technology Akure, School of Engineering and Engineering Technology, PMB 704, Ondo State, Nigeria
[1]mogajits@gmail.com

[2]Abdullahi O. Olapojoye
[2]Department of Mechanical Engineering, Federal University of Technology Akure, School of Engineering and Engineering Technology, PMB 704, Ondo State, Nigeria
[2]aolapojoye@yahoo.com

[3]Emmanuel T. Idowu
[1]Department of Mechanical Engineering,
Federal University of Technology Akure,
School of Engineering and Engineering Technology,
PMB 704, Ondo State, Nigeria
[3]Eiidowu21@yahoo.com

***Abstract*—This paper presents report on a Computational Fluid Dynamics (CFD) investigation on heat transfer enhancement characteristics of turbulent flow inside an internally helical grooved tubes with different pitch size (19, 57, and 95 mm) fitted with twisted tape inserts (twist ratio 3, 9, and 14). The simulations were performed in the Reynolds number range of 12000-22000 using water as the working fluid. The result from this study generally revealed that the enhanced tube independent of tested twist ratio and pitch size provided better thermal-hydraulic performance than their plain tube counterpart. Among the twist ratio tested, twist ratio of y =3 subjected to a moderate increment of the groove pitch size exhibited heat transfer augmentation up to 37% in comparison to the plain tubes without inserts. Evaluation of thermal performance factor revealed that the use of the choice heat transfer enhancement technique explored in this study is more efficient when it is applied to the lower Reynolds number region of the evaporator. The heat transfer performance of helical grooved tubes containing twisted tapes investigated in this work revealed that the CFD simulations can be used to improve future design considerations of heat exchanger devices, which would lead to improvement of thermal system efficiency.**

Keywords—grooved pitch; twisted ratio; thermal performance factor; heat transfer enhancement; CFD simulation.

Nomenclature

m_f	Mass flow rate
C_p	Specific heat of water
T_o	Outlet temperature
T_i	Inlet temperature
v	Fluid velocity
l	Length of tube, m
d_i	Internal diameter
λ	Thermal conductivity, W m^{-1} K^{-1}
T_f	Fluid bulk temperature, K
T_w	Average wall temperature, K
f	Friction factor
h	Convective heat transfer coefficient, W m^{-2} K^{-1}
Nu	Nusselt number
Δp	change in pressure drop, Pa
Re	Reynolds number
u	mean velocity, m s^{-1}
u_i'	fluctuation velocity components, m s^{-1}
Greek symbols	
μ	kinematic viscosity, kg $s^{-1}m^{-1}$
μ_t	eddy viscosity, kg $s^{-1}m^{-1}$
η	thermal performance factor
ε	turbulent dissipation rate, m^2 s^{-3}
ρ	density, kg m−3
δ_{ij}	Kronecker delta
φ	Dissipation function

1.0 INTRODUCTION

The demand for improving the efficiency and compactness of the thermal device has led to the development of various heat transfer enhancement techniques. Heat exchangers are known to have a major role in energy conservation in thermal engineering applications. Thus, it is necessary to improve their performance in order to save energy, cost, and material and to reduce environmental degradation. [1] pointed out that in recent years, the study of different techniques of heat transfer enhancement in heat exchanger devices has gained valuable attention and much research has been done. Heat exchangers are extensively used in HVAC systems (heating, ventilating and air conditioning), chemical and power plants, refrigeration systems, petroleum plants, etc. Most of the heat exchangers have the potential to be considered for heat transfer enhancement, however, each potential application should be tested to see if the enhancement is practical. According to [2], nearly all heat transfer enhancement techniques are used for heat exchangers in the refrigeration and automotive industries. Findings from studies of [3,4,5,6,7] have also proved that applying heat transfer enhancement techniques improves thermal performance significantly. However, increasing the rate of enhancement is at the penalty of pressure drop. Therefore, in any heat exchanger augmentation design, the heat transfer coefficient and pressure drop need to be critically analyzed. As pointed out in the study of [2] heat transfer augmentation can be carried out passively, actively and a combination of two or more of the aforementioned methods referred to as compound heat transfer enhancement technique. Heat transfer enhancement by the passive technique can be achieved by using coated or treated surfaces; displaced enhancement devices; swirl flow devices e.g. twisted tape inserts, vortex generator, static mixer and additives for liquids and gases. Active techniques need external power to promote the heat transfer rate. Active techniques are complicated due to the design and higher cost of the devices in comparison with passive methods. Therefore, their application is limited. With the view to maximize the usage of the aforementioned heat transfer enhancement techniques, the compound augmentation technique is investigated on by [4] which is a combination of more than one enhancement method (either from active or passive) to improve the thermal performance of heat exchanger devices. The choice of this type of enhancement technique is considered for investigation using CFD simulation in this work. Graham et al. [5] investigated the performance of an enhanced tube with helical angle of 0 using R134a as working fluid and compared results with a tube that has a helix angle of (18°) at different mass fluxes. The 18° helix angle tube performed better than the axially grooved tube. Heat performance factors showed an improvement in enhancement up to 62% and 20% for helical and axially grooved tubes compared to plain tubes at lower mass fluxes.

The effect of varying pitch lengths in grooved tubes on heat transfer was experimentally investigated by Aroonrat et al [8]. The authors observed a significant increase in the Nusselt number and friction factor obtained from enhanced tubes compared to that of the plain tube. Also, a decrease in the pitch length resulted in an increase in the Nusselt number and friction factor. Bilen et al. [6] experimentally investigated the effect of varying groove dimensions on heat transfer and pressure drop of turbulent flow in grooved tubes. Heat transfer augmentation up to 63% for circularly grooved, 58% for trapezoidal grooved and 47% for rectangular grooved was recorded, compared to plain tubes. Also, the correlation equation is developed experimentally for Nusselt number and friction factor for each tube. In the range of Reynolds between 10000 to 38000, thermal performance factor (η) for all grooved pipes is in the range of 1.24 to 1.28 for circularly grooved, 1.22 to 1.25 and 1.13 to 1.26 for trapezoidal and rectangular grooves respectively at constant pumping power.

Eiamsa-Ard et al. [7] carried out a numerical simulation to investigate the swirling flow of convective heat transfer in circular tubes with tight-fit (clearance = 0) twisted tapes and loose-fit (clearance > 0) twisted tapes. The best thermal performance factor at constant pumping power was observed for the tight-fit (CR = 0) clearance twisted tape type in their study. The numerical investigation was also conducted by [9] on the heat transfer and fluid flow of water through a circular tube with different tape inserts. All the shapes cut on the twisted tape insert have the same area, while twist ratio and tape thickness were also the same for each twisted tape. Their investigation revealed that the shape of cuts has effects on the performance of the twisted tapes, with alternate-axis triangular cut having the best performance. Bharadwaj et al. [10] applied the compound technique of heat transfer augmentation with a constant wall heat flux for water flow in an internally spiral grooved tube fitted with twisted tape inserts. Different twist ratios were considered for their study. Heat transfer augmentation up to 400% in laminar flow and 140% in turbulent flow was obtained for internally spiral grooved tubes compared with plain tubes. The addition of twisted tape inserts to an internally spiral grooved tube increased the augmentation to 600% for laminar and 140% for turbulent flow. However, in both cases, heat augmentation showed a decrease in the region $2000<Re< 13000$. Twist ratio of $y = 7.95$ exhibited the highest performance among the twist ratios tested.

Despite the numerous experimental works that have been carried out to investigate the performance of enhanced tubes, they are still limited in making optimum design judgement with geometrical variations due to equipment cost and time involved in carrying out such experiments. Moreover, a compound method whereby twisted tape is fitted into rectangular helical grooved tube is still scarcely researched on in the open literature. Besides, heat transfer enhancement techniques, modes of heat transfer and geometry classification are important. In this study, the single-phase flow with forced convection mode for the flow inside internally helical grooved tubes containing twisted tapes was considered. This study focused on the effect of groove pitch and twisted tape on heat transfer and the accompanying pressure drop. Groove geometry acts as roughness and promotes the flow mixing and interrupts boundary layers while the twisted tape insert creates secondary flow and increase swirl flow.

2.0 PHYSICAL AND MATHEMATICAL MODELS

2.1.1 Physical model

In this study, all models were generated in the Design-Modeler which is a component of ANSYS CFD FLUENT. Geometry modelling started with a 2D sketch shown in Figure 1which is defined by numeric and geometric parameters. With this software, parts and assemblies were created for both simple and complex geometry purposes. Detailed in the table below is the description of the models used in this study. PT stands for plain tube and GTT stands for Grooved tube containing twisted tape.

Table1: Geometric model Description

TUBE	Twist Ratio	Groove Width(mm)	Groove Depth(mm)	Length (mm)	Internal diameter (mm)	Pitch Length(mm)
PT				540	19	
GT1T14	14	1	1	540	19	19
GT1T9	9	1	1	540	19	19
GT1T3	3	1	1	540	19	19
GT3T14	14	1	1	540	19	57
GT3T9	9	1	1	540	19	57
GT3T3	3	1	1	540	19	57
GT5T14	14	1	1	540	19	95
GT5T9	9	1	1	540	19	95
GT5T3	3	1	1	540	19	95

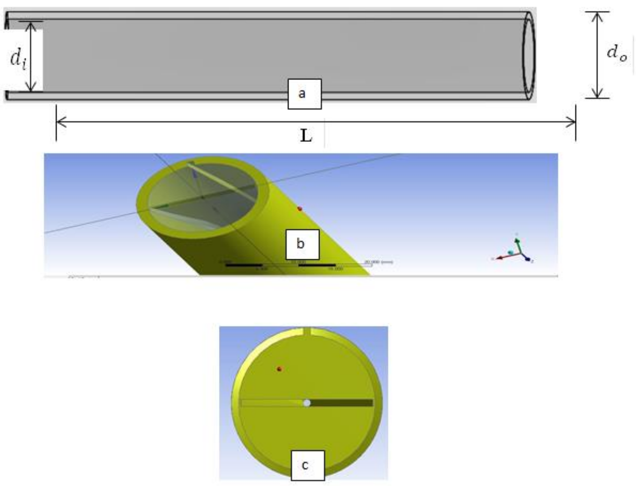

Figure.1: Geometry of current study (a) plain tube (b) inside view of grooved tube containing twisted tape (c) inlet view of grooved tube containing twisted tape.

2.1.2 Governing equations

For a three-dimensional models with water flowing in the tube considered to be incompressible and in steady-state, and having uniform velocity distribution adopted at the inlet and turbulent, it was assumed that: density of fluid is kept constant, fluid is incompressible, isotropic, Newtonian and thermal radiation, chemical reaction, compression work and effect of gravity are negligible. Also, since the fluid flowing inside the tube is considered to be fully developed turbulent flow, the Reynolds Averaged Navier-Stokes equations and the averaged energy equation are employed. The continuity, momentum and energy equations and turbulence models are given as follows:

Continuity equation: $\frac{\partial \rho}{\partial t} + \nabla.(\rho v) = 0$ (1)

Momentum equation:

$$\rho\left(\frac{\partial u}{\partial t} + u\frac{\partial u}{\partial x} + v\frac{\partial u}{\partial y} + w\frac{\partial u}{\partial z}\right) = \rho g_x - \frac{\partial p}{\partial x} + \mu\left[\frac{\partial^2 u}{\partial x^2} + \frac{\partial^2 u}{\partial y^2} + \frac{\partial^2 u}{\partial z^2}\right] \quad (2)$$

$$\rho\left(\frac{\partial v}{\partial t} + u\frac{\partial v}{\partial x} + v\frac{\partial v}{\partial y} + w\frac{\partial v}{\partial z}\right) = \rho g_y - \frac{\partial p}{\partial y} + \mu\left[\frac{\partial^2 v}{\partial x^2} + \frac{\partial^2 v}{\partial y^2} + \frac{\partial^2 v}{\partial z^2}\right] \quad (3)$$

$$\rho\left(\frac{\partial w}{\partial t} + u\frac{\partial w}{\partial x} + v\frac{\partial w}{\partial y} + w\frac{\partial w}{\partial z}\right) = \rho g_z - \frac{\partial p}{\partial z} + \mu\left[\frac{\partial^2 w}{\partial x^2} + \frac{\partial^2 w}{\partial y^2} + \frac{\partial^2 w}{\partial z^2}\right] \quad (4)$$

Energy equation:

$$\rho c_p \frac{DT}{Dt} = \nabla.k\nabla T + \mu\varphi \quad (5)$$

$$\varphi = 2\left[\left(\frac{\partial u}{\partial x}\right)^2 + \left(\frac{\partial v}{\partial y}\right)^2 + \left(\frac{\partial w}{\partial z}\right)^2\right] + \left(\frac{\partial u}{\partial y} + \frac{\partial v}{\partial x}\right)^2 + \left(\frac{\partial v}{\partial z} + \frac{\partial w}{\partial y}\right)^2 + \left(\frac{\partial w}{\partial x} + \frac{\partial u}{\partial z}\right)^2 \quad (6)$$

From literature, no single turbulence models can satisfactorily and reliably predict all turbulent flows with sufficient accuracy. Hence to obtain the optimum prediction of turbulence, the accuracy of two different turbulence models were mostly adopted to give better performance, which are: Realisable $k-\varepsilon$ model and RNG $k-\varepsilon$ model. Each of these models predicted good performances as earlier reported differently by researchers for fluid flow in tubes, but the realisable $k-\varepsilon$ model was often preferred to the RNG $k-\varepsilon$ model as it gave better performance between the two models as reported in the studies of [8; 11; 12]. Given this, the realisable $k-\varepsilon$ model was adopted in this study. In the realisable $k-\varepsilon$ model, two additional equations are solved for the transport of Turbulent Kinetic Energy (TKE) and turbulent dissipation rates and are given in Eqns. (7) and (8) as follows:

Turbulent kinetic energy, k

$$\frac{\partial}{\partial t}(\rho k) + \frac{\partial}{\partial x_j}(\rho k u_j) = \frac{\partial}{\partial x_j}\left[\left(\mu + \frac{\mu_t}{\sigma_k}\right)\frac{\partial k}{\partial x_j}\right] + G_k - \rho\varepsilon \quad (7)$$

Turbulent energy dissipation, ε

$$\frac{\partial}{\partial t}(\rho\varepsilon) + \frac{\partial}{\partial x_j}(\rho\varepsilon u_j) = \frac{\partial}{\partial x_j}\left[\left(\mu + \frac{\mu_t}{\sigma_\varepsilon}\right)\frac{\partial \varepsilon}{\partial x_j}\right] + \rho C_1 S\varepsilon - \rho C_2\frac{\varepsilon^2}{k+\sqrt{v\varepsilon}} \quad (8)$$

The term G_k in Eqn. (7) represents the production of turbulent kinetic energy and is given by

$$G_k = -\rho\overline{u_i' u_j'}\frac{\partial u_j}{\partial x_i} \quad (9)$$

The Reynolds stresses are appropriately modelled by a method that employs Boussinesq hypothesis to relate Reynolds stresses to the mean velocity gradients given as:

$$-\rho\overline{u_i'u_j'} = \mu_t\left(\frac{\partial u_i}{\partial x_j} + \frac{\partial u_j}{\partial x_i}\right) - \frac{2}{3}\left(\rho k + \mu_t\frac{\partial u_k}{\partial x_k}\right)\delta_{ij} (10)$$

The eddy viscosity is given by

$$\mu_t = \rho C_\mu \frac{{k_1}^2}{\varepsilon} (11)$$

The turbulent model constants in the realisable $k-\varepsilon$ model is expressed as follow:

$$C_1 = max\left[0.43, \frac{\eta}{\eta+5}\right], \qquad \eta = S\frac{k_1}{\varepsilon}, \qquad S \equiv \sqrt{2S_{ij}S_{ij}},$$

$C_2 = 1.9$, $\sigma_k = 1$, $\sigma_\varepsilon = 1.2$

The term S_{ij} represents the rate of linear deformation of a fluid element extracted from previous study of [13] and is express as:

$$S_{ij} = \frac{1}{2}\left(\frac{\partial u_i}{\partial x_j} + \frac{\partial u_j}{\partial x_i}\right) (12)$$

Where: $\bar{u}_i$ is the mean values of velocity and u' are fluctuating components, G_k represents the generation of turbulence kinetic energy due to the mean velocity gradients, $\sigma_k$turbulent Prandtl number for k, σ_ε turbulent Prandtl number for ε, $\sigma_{h,t}$ turbulent Prandtl number for energy and μ_t is the turbulent viscosity.

2.2 Boundary conditions

The physics model of liquid water is assumed to be incompressible, turbulent, three dimensional, steady in state and constant in density. Based on the turbulent model, some other related models should be activated too. When these physical models are assigned, they provide relevance to the transport energy and dissipation equations and semi-empirical coefficients for the solvers. After choosing a physical model, boundary condition and the initial value was set up. The outlet and inlet temperatures were acquired by mass flow average temperature in ANSYS CFD FLUENT which typically is calculated over the cross-section of the inlet and outlet of the tube by considering mass flow rate and radial temperature profile at the relevant section. This method provides a more accurate average temperature for flow which is called mean bulk temperature [14]. Thus, the mean velocity for the fluid flow presented in Table 2 is estimated using Eqn. (13):

$$\mathrm{Re} = \frac{\rho V d_h}{\mu} (13)$$

Table 2. Reynolds number (Re) and mean velocity of fluid (V) for plain tube

Re	12 000	14 000	16 000	18 000	20 000	22 000
V [m/s]	0.5413	0.6315	0.7217	0.8119	0.9021	0.9923

2.3 Physics of Simulation

The heat gained by the water inside the tube is calculated by the following energy conservation equation given as follows:

$$Q = m_f C_p (T_o - T_i) (14)$$

Where:m_f represent mass flow rate of water at inlet;$C_p$is the specific heat of water; T_o is outlet temperature; T_i represents the Inlet temperature.

Convective heat transfer is given by;

$$Q_c = h \times A \times (T_w - T_f) (15)$$

Where: h represents heat transfer coefficient; A is the cross-sectional area; T_f represents fluid bulk temperature; T_w represents Average wall temperature.

For a steady state condition, the convective heat transfer is equal to the heat transfer rate (i.e. $Q_c = Q$)

Therefore,

$$h = \frac{Q}{A \times (T_w - T_f)} (16)$$

$$N_u = \frac{h \times d_i}{\lambda} (17)$$

The friction factor was calculated from the relation given in Eqn. (18) as follows:

$$f = \frac{2 \times d_i \times \Delta p}{\rho \times l \times v^2} (18)$$

To determine the optimum condition at which the considered heat transfer enhancement device used in this work is profitable, the thermal performance factor relation is implored in analysing the obtained numerical simulation result in this study using Eqn. (19)

$$\eta = \left(\frac{Nu}{Nu_1}\right)\left(\frac{f}{f_1}\right)^{-1/3} (19)$$

Where: $Nu_1$and Nu are the Nusselt numbers for the plain tube and tube with insert respectively, andf_1 and f are friction factor for the plain tube and tube with insert respectively.

2.4 Solution procedure

A good simulation result depends on mesh quality, boundary conditions and computational model of the fluid. The procedure and guidelines to achieve these as detailed in the study of [15] were carefully adopted in this work. The numerical simulation was implemented using ANSYS release 14.5, commercial CFD software. The governing equations together were solved using a finite volume method (FVM) implemented in CFD code of ANSYS-FLUENT [13]. The FVM discretized the governing equations and the boundary conditions were applied. The computational domain was discretized using hexahedral elements with structured elements in the wall-normal directions. The coupling of pressure and velocity was done with SIMPLE (Semi Implicit Pressure Linked Equations) algorithm extracted from [14]. The scalable wall function was used for modelling the near-wall regions.

The convergence criterion was set to be satisfied when the values of the scaled residuals were in other of less than 10^{-4} for the continuity equation, less than 10^{-6} for velocity, turbulent kinetic energy and turbulent dissipation rate and less than 10^{-7} for energy.

3.0 RESULTS AND DISCUSSION

3.1 GRID INDEPENDENCE TEST AND VALIDATION OF SOLUTION PROCEDURE

3.1.1 Grid independence study and validation of smooth tube

Before starting to generate the CFD production runs, a mesh independence study was carried out for the plain tube with a diameter of 19mm and length of 540mm. According to [13], in a grid independence study, the goal was to find the best mesh properties for an accurate solution. The process is to vary the mesh density to eventually provide a desired numerical accuracy for engineering purposes at the same time achieving an optimized computational time. In this study, four different mesh densities were generated for a 19mm tube in ANSYS CFD and models were solved by the software. The final results of the obtained heat transfer variables such as outlet temperature and pressure drop were compared with each other in all cases and the results showed small differences by varying the mesh density. Therefore, based on the results, the solution was concluded to be independent of the number of cells. The grid generation started with a coarse mesh and followed by the refined mesh size type. The mesh density on inlet cross-section for different mesh densities is shown in Fig.2. The simulation is solved for a fluid region with the inlet velocity of 0.5413 m/s (Re=12000) and with constant wall temperature of 350K which was applied on the outer surface of the tube. The coarse mesh has 547694 cells, and then the numbers of cells were refined to three other meshes, 701684, 949494, and 1404424 respectively. Table 3 shows the result for grid independence test of plain tube model with the different number of elements, compared to estimated results from well-established single-phase heat transfer coefficient predictive method by Dittus-Boelter (D) [17] and Gnielinski (G) [18] respectively. Based on the comparisons displayed in Fig.3, it can be concluded that most of the simulated heat transfer data were reasonably predicted by the considered predictive methods from the literature. A similar analysis was performed for the friction factor predictive method by Petukhov (P) [19] and Blasius (B) [20] respectively. The comparison results of friction factor with four different grid sizes are presented in Fig.4. These comparisons, displayed in Fig. 4 shows that the simulated data agree quite well with the predicted values.

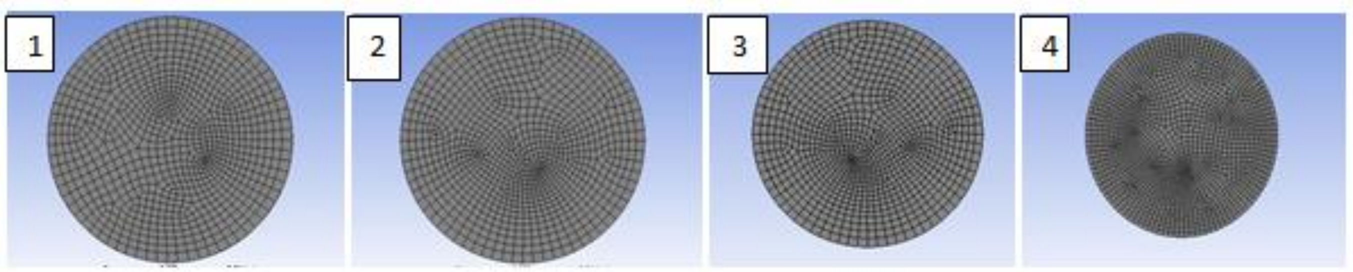

Figure 2: Mesh density (1) Mesh1 (2) Mesh2 (3) Mesh3 (4) Mesh4

Table. 3. Grid independence test of plain tube

Mesh	Grid size	T_{out} (K)	ΔP	Nusselt Number				Friction Factor			
				Correlation results		CFD	%Diff	Correlation results		CFD	%Diff
Mesh1	547694	306.8	128.3	G	90.90	89.08	2.00	P	0.0293	0.0309	5.18
				D	87.86	89.08	1.37	B	0.0296	0.0309	4.21
Mesh2	701684	306.7	127.4	G	90.90	88.94	2.16	P	0.0293	0.0307	4.56
				D	87.86	88.94	1.21	B	0.0296	0.0307	3.58
Mesh3	904424	306.7	127.6	G	90.90	88.90	2.20	P	0.0293	0.0307	4.56
				D	87.86	88.90	1.17	B	0.0296	0.0307	3.58
Mesh4	1449494	306.8	127.9	G	90.90	89.08	2.00	P	0.0293	0.0309	5.02
				D	87.86	89.08	1.37	B	0.0296	0.0309	4.05

Journal of Multidisciplinary Engineering Science Studies (JMESS)
ISSN: 2458-925X
Vol. 6 Issue 2, February - 2020

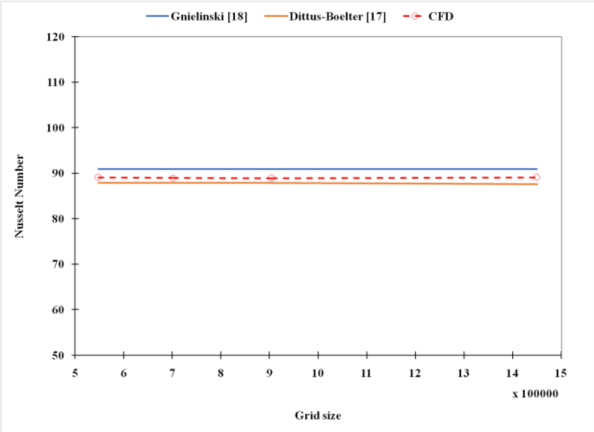

Figure 3: Grid Independence test of Nusselt number for plain tube flow.

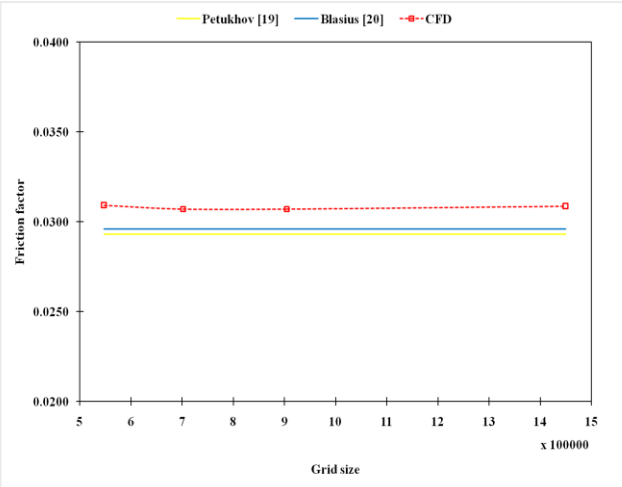

Figure 4: Grid Independence test of friction factor for plain tube flow.

3.1.2 Grooved Tubes Validation

Experimental study of [8] for tubes with an internal helical groove and pitch distance of 203, 254 and 305mm is considered for validation with the present study simulation generated data as presented in Figs.5 and 6. Based on the comparisons displayed in Figs.5 and 6, it can be concluded that most of the simulated heat transfer and friction factors were predicted within an error band smaller than ±10%. The agreement between experimental results and CFD simulation results is considered satisfactory, thus the CFD model in this work can be used for expanding the study for different diameter, pitch \sizes and Re number of various ranges.

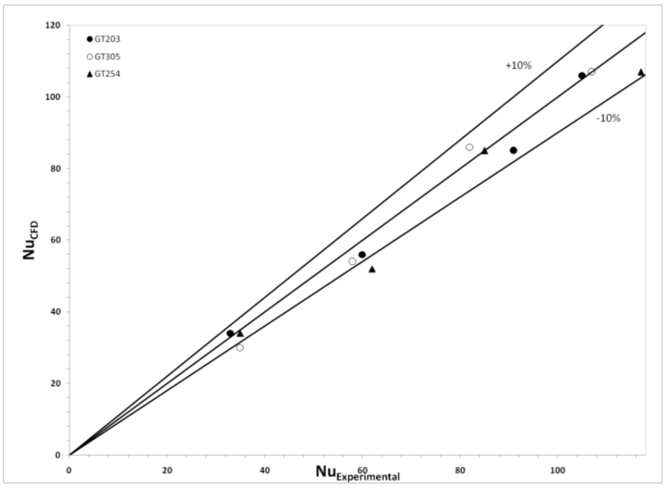

Figure 5: Comparison between the Experimental result of [8] and CFD simulated Nusselt Number

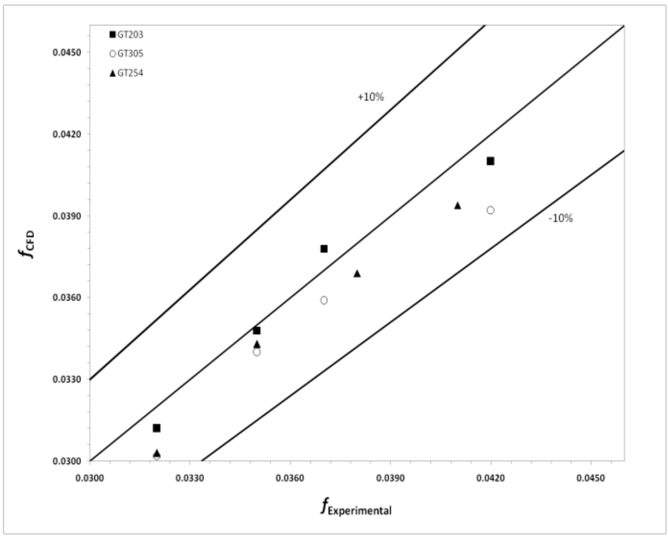

Figure 6: Comparison of the experimental result of [8] with CFD simulated friction factors

3.1.3 Effect of twisted tape inserts and grooved pitch size on Nusselt number

The effect of twisted tape inserts inside internally helical grooved tubes on Nusselt number as a function of Reynolds number results for the tested three twist ratios and three groove pitches are shown in Fig.7 and contour plots in Fig.8. The same constant wall temperature of 350 K applied on the tube surface and Reynolds number for each tube with tape inserts is varied from 12000 to 22000. The Nusselt number is calculated using Eq. (17). Result from Figure 7 shows that the Nusselt number increases with Reynolds numbers from 12000 to 22000. It can also be observed that as the twist ratio decreases, there is an increase in turbulence/ swirl flow of the fluid caused by the inserted tape and hence the enhanced tube yielded better heat transfer enhancement of up to 37% compared to the plain tube without inserts counterpart.

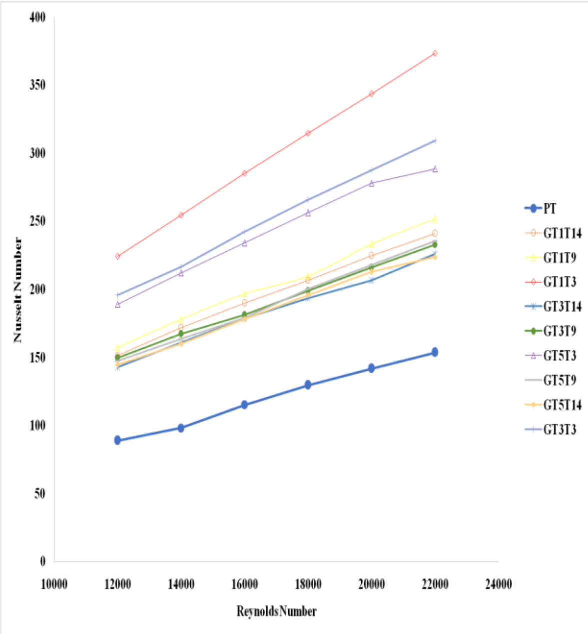

Figure 7: Evolution of Nusselt number as a function of Reynolds number for grooved tubes fitted with twisted tapes and plain tube.

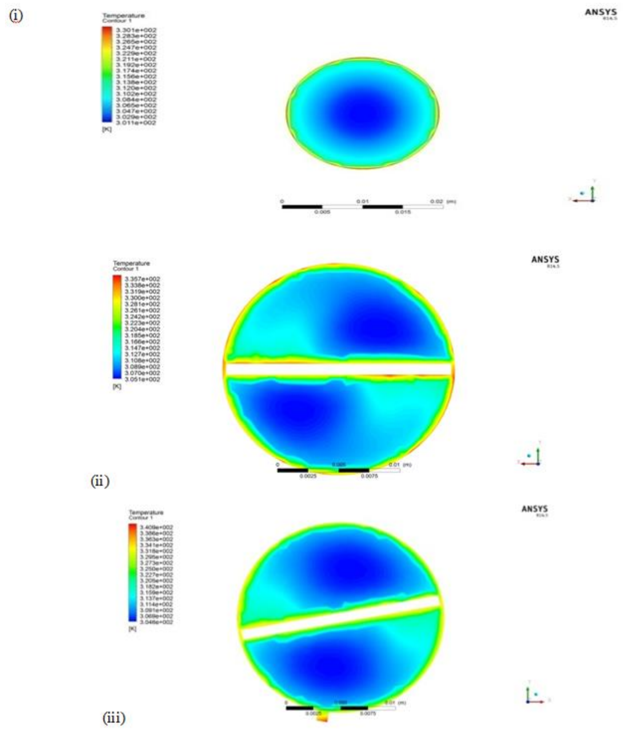

Figure 8: Outlet temperature contours for (i) plain tube (ii) plain tube containing twisted tapes (iii) grooved tube containing twisted tape

3.1.4Effect of twisted tape inserts and grooved pitch on friction factor

Presented in Figure 9 and contour plots in Figure 10 is the variation of friction factor as a function of Reynolds number ranging from 12000 to 22000. From the figure it is observed that the f values for water flowing in the helical grooved tubes containing twisted tape inserts decrease monotonically with increasing Reynolds number, indicating that the choice heat transfer enhancement method in this work compared to the plain tube counterpart causes an increase in swirl flow and recirculation around these grooves resulting to an increased f. This behaviour is observed to be more pronounced with the use of smaller twist ratio and pitch size values considered under the same operational condition. These results agree with the typical behaviour observed in those reported in the study of [14;21].

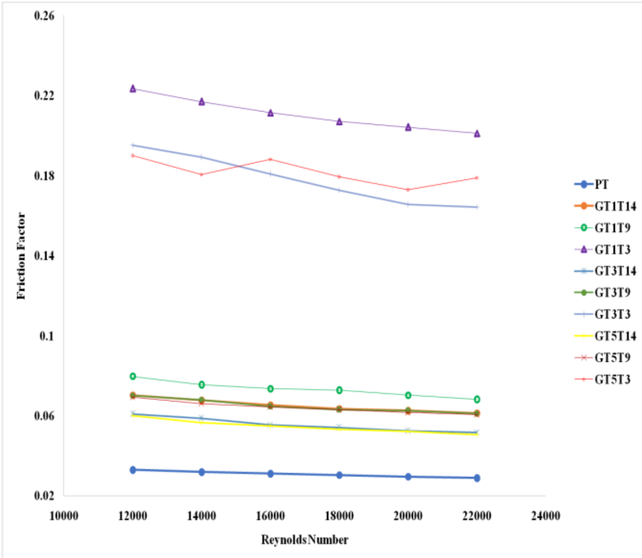

Figure 9: Evolution of friction factor as a function of Reynolds number for grooved tubes fitted with twisted tapes and plain tube

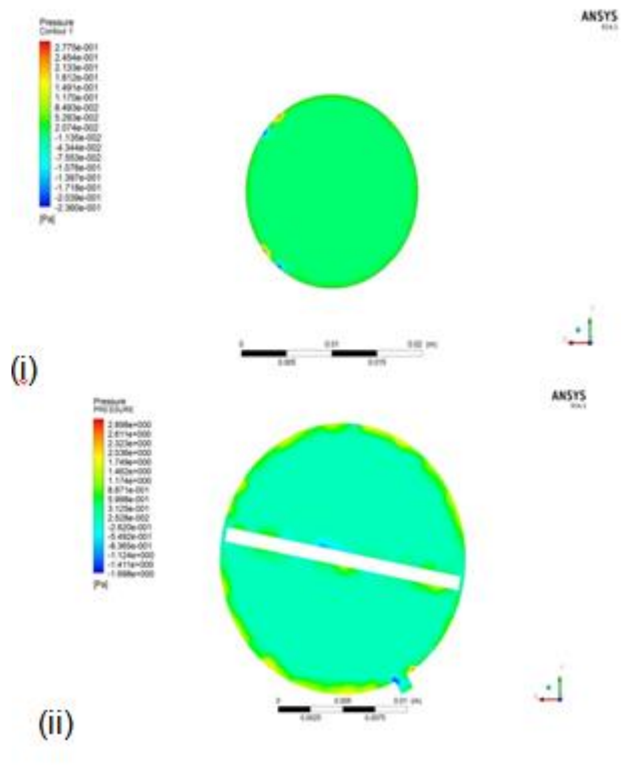

Figure 10: Pressure Contours (i) Plain tube (ii) Grooved tube containing twisted tape inserts

Figure 11 shows a comparison between the CFD numerical data of the current study and the experimental results of [10] for Nusselt Number of single-phase flows in helical grooved tubes containing twisted tape inserts. The author carried out heat transfer and pressure drop investigation in a spirally grooved tube with twisted tape insert with twist ratios 10.16, 7.95 and 3.4. Even though there were differences in the dimensions of the grooves and the twist ratios considered in the study of [10], the rate of heat transfer followed the same trend as depicted in Figure 11. The CFD numerical f values data from this study were also compared with the experimental f values obtained by [6] as displayed in Figure 12. The author [6] in their study evaluated the effects of circular, rectangular and trapezoidal grooves on friction factor. The present study focused on varying groove pitch and other groove geometric parameters such as depth, width and helix angle in helical grooved tubes containing twisted tape inserts. It can be noticed that both CFD numerical f values result from this study and the experimental f values obtained by [6] follow the same trend. The observed variation between the f values results of this work and that of [6] may be due to different geometric parameters considered in their study.

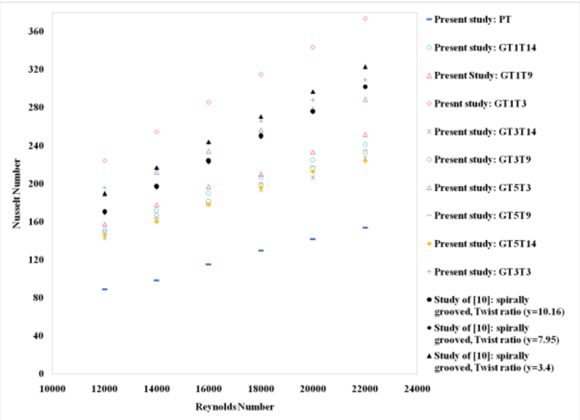

Figure 11: Comparison between the numerical results of current study and the experimental results of [10] for Nusselt Number.

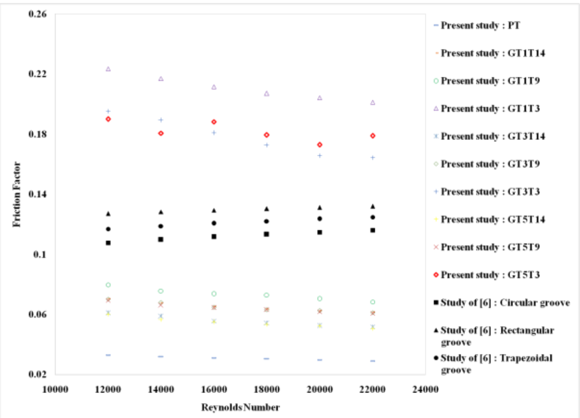

Figure.12. Comparison between the numerical results of current study and the experimental results of [6] for friction factor.

4 OVERALL PERFORMANCE OF THE HEAT TRANSFER ENHANCEMENT TECHNIQUE

In general, momentous turbulence is promoted as a result of geometric modifications and twisted tape inserts aspect of compound enhancement technique considered in this work, but there is a penalty of increased pressure drop and pumping power that comes with it. To determine the optimum condition at which the considered heat transfer enhancement devices used in this work is profitable, the thermal performance factor, □, relation given in Eq. (19) is implored. This parameter, □, is defined as the ratio of the Nu number of grooved tubes containing twisted tape to a plain tube over the friction factor ratio of grooved tubes containing twisted tape inserts to a plain tube. Figure 13 shows the η of the studied cases as a function of Re number. According to San and Huang (2006), if the □≥1, it reflects that the increase in heat transfer is more or about the same as the increase in friction factor indicating that the tube design is efficient to be used for enhancement purposes. This behaviour is observed to be more pronounced at the lower region of the tube in this work for Reynolds number value of 14000, thus attained highest □=1.37 for the tape insert of twist ratio of T3 with GT1 (pitch size of 19 mm). Since the highest enhancement factor for all compound enhanced tubes investigated occurred at Re number of 14000 thus, the Re of the 14000 is a critical point for enhancement factor in the current work. It is also noticed that □>1 was attained for the range of 12000 to 22000 considered in this study independent of the twist ratio and the groove pitch size considered. This result established that the internally helical grooved tube with tape inserts investigated in this study is efficient to enhance thermal performance in heat exchanger devices.

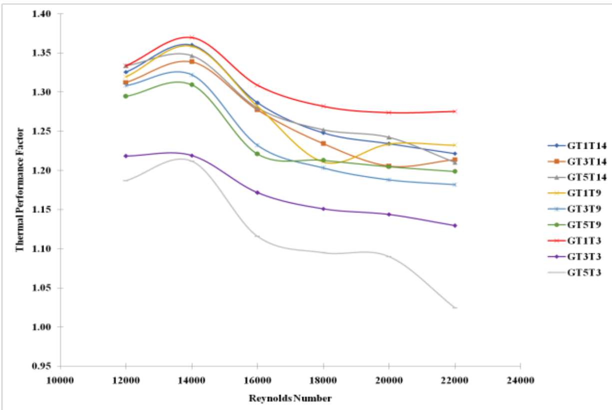

Figure 13: Thermal Performance factor as a function of Reynolds Number for three different grooved tubes.

5 CONCLUSIONS

The CFD study on heat transfer enhancement characteristics of water flowing inside grooved tubes with different pitch size (19, 57, and 95 mm) fitted with twisted tape inserts (twist ratio 3, 9, and 14) was evaluated in this study. The following conclusions can be drawn from the present study.

- The Nusselt number and friction factors curves obtained for water flowing inside grooved tubes fitted with twisted tape inserts and plain tubes without insert follow the general trend pointed out in the literature.
- The Nusselt number and friction factors obtained from current CFD works for an internally helical grooved tube containing twisted tapes were higher than those obtained from plain tubes. This is due to an increase in turbulence caused by inducing of swirl flow by the inserted twisted tape.
- By implementing the compound enhancement technique in this work, heat transfer coefficient enhancements of up to 37%, were observed in comparison to heat transfer coefficient values for the plain tubes.
- For the tape insert of twist ratio 3 subjected to a moderate increment of the groove pitch size, appreciable enhancement of the heat transfer coefficient was observed for the enhanced tubes as compared to the plain tube counterpart. It is argued that this phenomenon is related to the swirling flow and efficient mixing of the fluid caused by the inserted twisted tape and the choice groove pitch size.
- The analysis of the thermal enhancement factor allowed concluding that the use of the choice compound enhancement technique investigated in this study is more efficient when it is applied to the lower Reynolds number region of the evaporator.

ACKNOWLEDGMENTS

The authors would like to acknowledge the assistance of the Refrigeration and Air Conditioning Unit of the Department of Mechanical Engineering, Federal University of Technology Akure in supplying the needed information used in the present study.

COMPETING INTERESTS

Authors has declared that no competing interests exist.

REFERENCES

[1] K. Manjunath and S. C. Kaushik, (2014). Second law thermodynamic study of heat exchangers: A review, *Renewable and Sustainable Energy Reviews*, 40, 348–374.

[2] R. L. Webb, and N. H. Kim, (2005), Principles of Enhanced Heat Transfer (2nd ed.), New York: Taylor & Francis.

[3] S. Liu, and M. Sakr, (2013) A comprehensive review on passive heat transfer enhancements in pipe exchangers, Renewable and Sustainable Energy Reviews, 19, 64–81.

[4] G. Johar and V. Hasda, (2010) Experimental studies on heat transfer augmentation using modified reduced width twisted tapes (RWTT) as inserts for tube side flow of liquids. Thesis, Department of Chemical Engineering, National Institute of Technology Rourkela.

[5] D. Graham, J. C. Chato, T. A. Newell, (1999), Heat transfer and pressure drop during condensation of refrigerant 134a in an axially grooved tube, *International Journal of Heat and Mass Transfer,* 42,1935-1944.

[6] K. Bilen, M.,Cetin, H. Gul, T. Balta, (2009), The investigation of groove geometry effect on heat transfer for internally grooved tubes, *Applied Thermal Engineering,* 29, 753–761.

[7] S. Eiamsa-Ard, K. Wongcharee S. Sripattanapipat, (2009) 3D Numerical Simulation of Swirling Flow and Convective Heat Transfer in a Circular Tube Induced by Means of Loose-fit Twisted Tapes, International Communications in Heat and Mass Transfer 36:947–955

[8] K. Aroonrat, C. Jumpholkul, R. Leelaprachakul, A.S. Dalkilic, O. Mahian, and S. Wongwises, (2013) Heat transfer and single-phase flow in internally grooved tubes, International Communications in Heat and Mass Transfer, 42, 62–68.

[9] T.O Oni, M.C Paul (2016) CFD investigation of the impacts of variation in geometry of twisted tape on heat transfer and flow characteristics of water in tubes, Heat Transfer: Asian Research 45(5):482–498.

[10] P. Bharadwaj, A.D Khondge, A.W. Date, (2009), Heat transfer and pressure drop in a spirally grooved tube with twisted tape insert, International Journal of Heat and Mass Transfer, 52, 1938–1944.

[11] A. Mwesigye, T. Bello-Ochende, J. P. Meyer (2016) Heat transfer and entropy generation in a parabolic trough receiver with wall-detached twisted tape inserts, International Journal of thermal Science 99:238–257.

[12] K. Ceylan and G. Kelbaliyev, (2003), The roughness effects on friction and heat transfer in the fully developed turbulent flow in pipes, *Applied Thermal Engineering*, 23, 557–570.

[13] S. Singh, B. Singh, V.S Hans, R.S Gill, (2015),CFD (computational fluid dynamics) investigation on Nusselt number and friction factor of solar air heater duct roughened with non-uniform cross-section transverse rib, *Journal of Energy* ,84, 509-517.

[14] S. D. Salman, A.A.H. Kadhum, M.S. Takriff, A .B. Mohamad, (2014),CFD Simulation of

[15] L.M Jiji, (2009). Heat Convection (2nd Ed.). Germany: Springer.

[16] Heat Transfer Augmentation in a Circular Tube Fitted with Alternative Axis Twisted Tape in Laminar Flow under a Constant Heat Flux, *Heat Transfer—Asian Research*, 43, 4

[17] F. W. Dittus, L.M.K, Boelter (1930): Heat transfer in automobile radiators of the tubular type, Univ. Calif, International Chemical Engineering 2:443–461.

[18] V. Gnielinski (1976): New equations for heat and mass transfer in turbulent pipe and channel flow, International Chemical Engineering 16 (2):35 –368

[19] B.S Petukhov (2015): "Heat transfer and friction in turbulent pipe flow with variable physical properties" in Advances in heat transfer, J.P. Hartnett

and T.F. Irvine, Jr., Editors. Academic Press: New York. pp 503-564

[20] H. Blasius, (1908): “Grenzschichten in flussigkeitenmitkleinerreibung,” Zeritschrift fur angewandteMathematik und Physik. 56:1–37.

[21] M. A. Elyyan, (2008). Heat Transfer Augmentation Surfaces Using Modified Dimples/Protrusions (Dissertation). Virginia Polytechnic Institute and State University, Virginia,